Cerebrovascular reactivity and white matter integrity

Kevin Sam, PhD
Boris Peltenburg, MD
John Conklin, MD, MSc
Olivia Sobczyk, MSc
Julien Poublanc, MSc
Adrian P. Crawley, PhD
Daniel M. Mandell, MD, PhD
Lakshmikumar Venkatraghavan, MD
James Duffin, PhD
Joseph A. Fisher, MD
Sandra E. Black, MD
David J. Mikulis, MD

Correspondence to Dr. Mikulis: mikulis@uhnres.utoronto.ca

ABSTRACT

Objective: To compare the diffusion and perfusion MRI metrics of normal-appearing white matter (NAWM) with and without impaired cerebrovascular reactivity (CVR).

Methods: Seventy-five participants with moderate to severe leukoaraiosis underwent blood oxygen level–dependent CVR mapping using a 3T MRI system with precise carbon dioxide stimulus manipulation. Several MRI metrics were statistically compared between areas of NAWM with positive and negative CVR using one-way analysis of variance with Bonferroni correction for multiple comparisons.

Results: Areas of NAWM with negative CVR showed a significant reduction in fractional anisotropy by a mean (SD) of 3.7% (2.4), cerebral blood flow by 22.1% (8.2), regional cerebral blood volume by 22.2% (7.0), and a significant increase in mean diffusivity by 3.9% (3.1) and time to maximum by 10.9% (13.2) ($p < 0.01$), compared to areas with positive CVR.

Conclusions: Impaired CVR is associated with subtle changes in the tissue integrity of NAWM, as evaluated using several quantitative diffusion and perfusion MRI metrics. These findings suggest that impaired CVR may contribute to the progression of white matter disease.
Neurology® 2016;87:2333–2339

GLOSSARY

ANOVA = analysis of variance; **BOLD** = blood oxygen level–dependent; **CBF** = cerebral blood flow; **CVR** = cerebrovascular reactivity; **DSC** = dynamic susceptibility contrast; **DTI** = diffusion tensor imaging; **FA** = fractional anisotropy; **FDT** = FMRIB Diffusion Toolbox; **FLAIR** = fluid-attenuated inversion recovery; **MD** = mean diffusivity; **MTT** = mean transit time; **NAWM** = normal-appearing white matter; **rCBV** = relative cerebral blood volume; **ROI** = region of interest; **SHSC** = Sunnybrook Health Sciences Centre; **TE** = echo time; **Tmax** = time-to-maximum; **TR** = repetition time; **TTP** = time-to-peak; **TWH** = Toronto Western Hospital; **WMH** = white matter hyperintensity.

Changes in the periventricular and subcortical white matter are observed on both CT and MRI scans of elderly individuals.[1] The affected areas appear hyperintense on T2-weighted MRI, and are labeled as white matter hyperintensities (WMHs) if they are of presumed vascular origin.[2] They are associated with an increased risk of dementia,[3] stroke,[4] and cognitive disability,[5] and correlated with age; as many as 95% of individuals over age 50 have WMHs.[6,7] Therefore, preventing or slowing the progression of WMHs has the potential to lower the disease burden. Although several modifiable risk factors have been associated with WMH progression, such as smoking and high blood pressure,[8] the detailed pathogenesis of WMHs remains controversial. Nevertheless, the prevailing view is that a chronic low-grade ischemic injury is the final common pathway for these lesions,[9,10] and this view was the motivation for our study.

Accordingly, this study characterized vascular pathophysiology in normal-appearing white matter (NAWM) before progression to overt leukoaraiosis by measuring cerebrovascular reactivity (CVR); the change in cerebral blood flow in response to a vasodilatory stimulus. Negative CVR values represent steal physiology, in which blood flow is redistributed from regions of exhausted cerebral vasodilatory reserve to areas with preserved vasodilatory capacity.[11] We

Supplemental data at Neurology.org

From the Department of Physiology (K.S., J.D., J.A.F.), Division of Neuroradiology, Joint Department of Medical Imaging, Toronto Western Hospital (K.S., J.C., O.S., J.P., A.P.C., D.M.M., D.J.M.), Department of Medical Imaging (A.P.C., D.M.M., D.J.M.), and Department of Anaesthesia, Toronto General Hospital (L.V., J.D., J.A.F.), The University of Toronto, Canada; Department of Radiotherapy (B.P.), Imaging Division, University Medical Center Utrecht, Utrecht University, the Netherlands; and L.C. Campbell Cognitive Neurology Research Unit (S.E.B.), Sunnybrook Health Sciences Centre, Toronto, Canada.

Go to Neurology.org for full disclosures. Funding information and disclosures deemed relevant by the authors, if any, are provided at the end of the article.

hypothesized that NAWM with steal physiology (negative CVR) would demonstrate quantifiable alterations in tissue microstructure and perfusion similar to preexisting areas of WMH, as assessed with diffusion tensor imaging (DTI) and dynamic susceptibility contrast (DSC) perfusion MRI. DTI and DSC MRI allow in vivo quantitation of alterations in white matter microstructure and perfusion, which may precede the development of frank WMH. Therefore, we evaluated the utility of negative CVR, a known biomarker of cortical vascular dysfunction,[12] as a marker for pathophysiology in 75 participants with age-related WMHs by comparing NAWM with negative CVR to contralateral spatially homologous NAWM with positive CVR.

METHODS

Participant recruitment and assessment. This 2-center study included participants from the Toronto Western Hospital (TWH) and Sunnybrook Health Sciences Centre (SHSC). Magnetic resonance angiography or CT angiography and T2-weighted fluid-attenuated inversion recovery (FLAIR) images of all patients were screened by experienced neuroradiologists (D.M.M., D.J.M.).

Patients were recruited from the outpatient neurology clinics at both institutions based on the following inclusion criteria: (1) no recent subcortical infarct involving the white matter (patients were excluded if they had a previous DWI-positive white matter infarct within the 3 months preceding study enrollment); (2) no prior cortical infarct >2 centimeters or cavitary white matter lesion >2 centimeters; (3) age >50 years; (4) white matter disease burden > Fazekas grade 2[13]; (5) no evidence of hemodynamically significant (>70%) internal carotid artery or vertebrobasilar stenosis; (6) no evidence of dissection; (7) no evidence of pulmonary or cardioembolic disease. Patients with motion artifacts on blood oxygen level–dependent (BOLD) images were excluded. Seventy-five patients (age range 50–91 years, mean age 73.3 years, 40 men and 35 women) with moderate to severe leukoaraiosis met the inclusion criteria and were considered in subsequent analyses. See the table for participant characteristics.

Table Baseline characteristics of participants

	Values (total n = 75)
Demographics	
Age, y, mean (SD)	74 (9.7)
Men, n (%)	40 (53)
Baseline WMH volume, mL, mean (SD)	27 (24)
MoCA (6 missing values), mean (SD)	24 (5)
Vascular risk factors, n (%)	
Ischemic stroke	26 (35)
TIA	14 (19)
CAD	11 (15)
Dyslipidemia	39 (52)
Hypertension	47 (63)
Diabetes mellitus	10 (13)
Current smoking	4 (5)
Obstructive sleep apnea	6 (8)

Abbreviations: CAD = coronary artery disease; MoCA = montreal cognitive assessment; WMH = white matter hyperintensities.

Standard protocol approvals, registrations, and patient consents. Research at TWH and SHSC was ethically conducted and approval was obtained from institutional review boards at the University Health Network and Sunnybrook Research Ethics Board, respectively. Written informed consent was obtained from all participants.

MRI acquisition. Participants underwent MRI scans on a 3T GE system (Signa HDx platform, GE Healthcare, Milwaukee, WI) at TWH and 3T Philips Achieva system (Philips Medical Systems, Best, Netherlands) at SHSC and were fitted with an 8-channel phased array head coil. Participants were asked to refrain from heavy exercise and consuming caffeine on the day of the scan. The imaging acquisition parameters were as follows, with values listed as SHSC/TWH: T1-weighted 3D spoiled gradient echo sequence (slice thickness 1.2 [SHSC]/1.5 [TWH] mm; no interslice gap; matrix size 256 × 256; field of view 22 × 22 cm; flip angle 8/20°; echo time [TE] 2.3/3 ms; repetition time [TR] 7.8/9.5 ms), BOLD fMRI using a T2*-weighted echoplanar imaging gradient echo sequence (slice thickness 3.0/5.0 mm; field of view 24 × 24 cm; matrix size 64 × 64; flip angle 85/90°; TE 30 ms; TR 2,000 ms), conventional FLAIR images (slice thickness 3 mm; 36–52 slices per volume; no interslice gap; matrix size 256 × 224/240 × 240; field of view 22 × 22 cm; flip angle 90°; TE 125/165 ms; TR 9,000/9,145 ms; inversion time 2,200/2,800 ms); diffusion tensor imaging with echoplanar imaging spin-echo sequence (slice thickness 3 mm; matrix size 76 × 62/128 × 128; field of view 22 × 22 cm; b = 1,000 s/mm^2; 23 diffusion-encoding gradients; 2 non-diffusion-weighted B0 images; TE 55/80 ms; TR 9,150/14,500 ms); proton density/T2-weighted images using fast spin echo-XL (slice thickness 3 mm; matrix size 128 × 128/256 × 209; field of view 22 × 22 cm; flip angle 90°; TE 11.1/90 to 11/102 ms; TR 2,500/7,200 ms), multiecho T2 mapping using a fast spin echo-XL (slice thickness 3 mm; no interslice gap; matrix size 256 × 192; field of view 230 × 184/22 × 22 cm; TE 13, 26, 39, 52, 65, 78, 91, 104, 117, 130, 143, 156 ms; TR 5,000/6,000 ms), and DSC perfusion scan using gradient-multiphase echo echoplanar imaging sequence (slice thickness 5 mm; matrix size 128 × 128; field of view 27 × 27 cm; flip angle 90°; TE 31.5 ms; TR 1,725 ms; 50 slices per location), during which a single dose of 0.1 mmol/kg of gadolinium contrast agent was injected at a rate of 5 mL/s.

CVR measurement. CVR was assessed by measuring the change in BOLD MRI signal in response to changes in the end-tidal (i.e., end expiratory) partial pressure of carbon dioxide ($P_{ET}CO_2$) as the vasoactive stimulus.[14] CVR was calculated as $\Delta\%BOLD/\Delta P_{ET}CO_2$.

Vasodilatory stimulus. To precisely manipulate carbon dioxide, we used an automated gas blender that adjusts the flow and gas composition to a sequential gas delivery breathing circuit (RespirAct, Thornhill Research Inc., Toronto, Canada) as previously described.[15,16] The system enables independent manipulation of end-tidal partial pressures of oxygen ($P_{ET}O_2$) and carbon dioxide ($P_{ET}CO_2$).[17,18] The stimulus sequence protocol used in this study was as follows: a baseline $P_{ET}CO_2$ of 40 mm Hg for 60 seconds (normocapnia), a step change in $P_{ET}CO_2$ from 40 to 50 mm Hg

for 90 seconds, a return to 40 mm Hg for 90 seconds, and a second hypercapnic step from 40 to 50 mm Hg for 120 seconds with a final return to baseline[17] normoxia ($P_{ET}O_2$ ~110 mm Hg) was maintained throughout.

Image reconstruction. BOLD MRI and $P_{ET}CO_2$ data were imported to AFNI[19] to generate CVR maps. Separate BOLD images were aligned to the same temporal origin, registered to the first volume, and then aligned to T1-weighted images. The acquired $P_{ET}CO_2$ contains a temporal discrepancy with the BOLD signal due to delay from pulmonary to cerebral circulation. To correct for this, the $P_{ET}CO_2$ data were temporally shifted to the point of maximum correlation with the whole brain average BOLD signal using MATLAB software. Finally, the BOLD time series was fitted to the $P_{ET}CO_2$ using a voxel-by-voxel linear least-squares fit. CVR was taken as the slope of the linear regression. CVR values are expressed as percent BOLD MRI signal change per mm Hg of $P_{ET}CO_2$.

To detect tissue dysfunction in the cerebral white matter, T2, reflecting white matter water content and myelination, was measured using a multi-echo fast spin-echo sequence. T2 maps were calculated using AFNI with methods previously described.[20] To calculate fractional anisotropy (FA) and mean diffusivity (MD) maps, diffusion-weighted images were imported into FSL 4.1.8 (www.ndcn.ox.ac.uk/divisions/fmrib) for quality control.[21] Preprocessing included eddy current and motion artifact correction using FMRIB's Diffusion Toolbox (FDT). Then, individual brain masks were created using Brain Extraction Tool.[22] The preprocessed images were fitted with a diffusion tensor model using DTIFIT in FDT.[21]

The time-signal attenuation curves obtained from perfusion-weighted T2* images were converted to time-concentration curves using PerfTool,[23] which uses a delay-insensitive, reformulated singular value decomposition approach to deconvolution of the time-concentration curves.[24] The arterial input function was selected from a region of interest (ROI) placed on the middle cerebral artery. The preprocessed perfusion-weighted images were used to generate maps of cerebral blood flow (CBF), relative cerebral blood volume (rCBV), mean transit time (MTT), time-to-maximum (Tmax), and time-to-peak (TTP) using PerfTool.[23]

Generating ROIs of WMH and NAWM. Segmentation of WMH was performed using the Lesion Explorer processing pipeline.[25,26] T1-weighted anatomical images were segmented into CSF, gray matter, and white matter using SPM8 (Wellcome Department of Imaging Neuroscience, Institute of Neurology, University College, London, UK). A diamond-shaped structuring element was used to erode the white matter segmentation in 5 iterations at the resolution of the T1-weighted image to prevent partial volume effects. The WMHs were subtracted after erosion to give rise to a NAWM mask (figure 1). To identify regions of steal physiology in NAWM, CVR maps were overlaid on the NAWM using AFNI (figure 2).

Accounting for the spatial factor confound. Differences between NAWM with positive and negative CVR may be subject to a spatial confound because (1) regions of negative CVR tend to be in close proximity to areas with WMH and (2) the CVR of white matter may be lower near the ventricles and higher near the cortical surface.[27] Consequently, masks of NAWM with negative CVR may include more periventricular voxels and masks of NAWM with positive CVR may include more voxels adjacent to cortex. It is therefore possible that the differences between NAWM with positive and negative CVR are just a reflection of the variable physiology in the neighboring WMHs, and so differences between NAWM masks may produce false-positive results. To account for these possible effects of spatial location, T1-weighted images were transformed into Montreal Neurologic Institute space using SPM8. The transformation matrix was then applied to the other MRI metrics, transforming these maps to a standard space but retaining the native structure. A second ROI of NAWM with positive CVR was generated, contralateral and spatially homologous to NAWM with negative CVR (figure 3). Comparison between these ROIs allows evaluation of the effect of CVR differences without potential confounding by spatial location.

Statistical analyses. WMHs were compared with 3 different groups of NAWM: (1) a mask containing the entire NAWM; (2) the entire NAWM segmented based on CVR; (3) NAWM with contralateral homologous regions defined in figure 3.

NAWM with positive CVR was compared against NAWM with negative CVR. MRI metrics in WMH were also compared to the entire NAWM using Friedman test with Dunn post hoc correction for multiple comparisons for nonparametric MTT data. Statistical analyses of all other MRI metrics involved repeated-measures one-way analysis of variance (ANOVA) using the MRI parameters as dependent variables and ROIs as the matched-pairs independent variable. Mauchly test was used to assess deviations from sphericity and degrees of freedom were

Figure 1 Identification of normal-appearing white matter (NAWM)

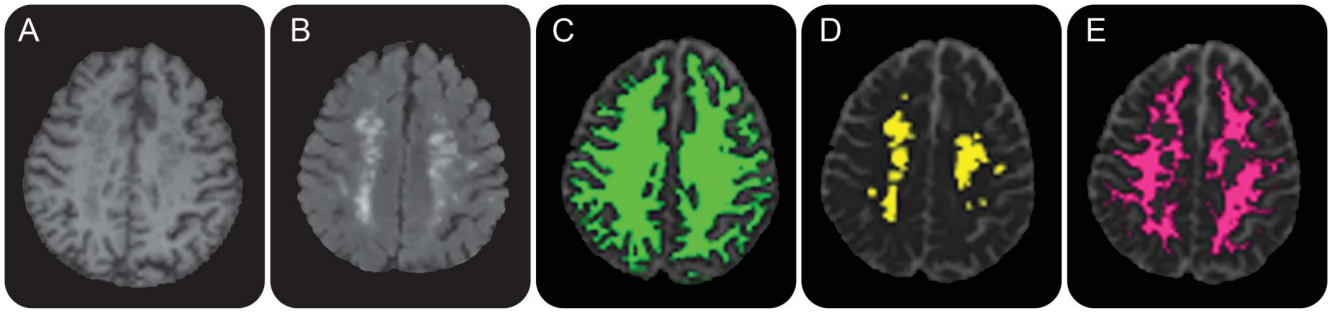

(A) Example of a T1-weighted image from a participant with diffuse periventricular and deep white matter hyperintensities (WMHs). (B) Fluid-attenuated inversion recovery images highlight the hyperintensities seen in this participant. (C) The white matter (green) was segmented from other subdural structures such as CSF and gray matter. (D) Regions of hyperintensities are identified in yellow. (E) NAWM mask: a diamond-shaped structuring element was used to erode the white matter (C) in 5 iterations at the resolution of the T1-weighted image (A) to account for partial voluming effects. The WMHs were subtracted after erosion to give rise to a final NAWM mask (pink).

Figure 2 Identification of normal-appearing white matter (NAWM) with steal physiology

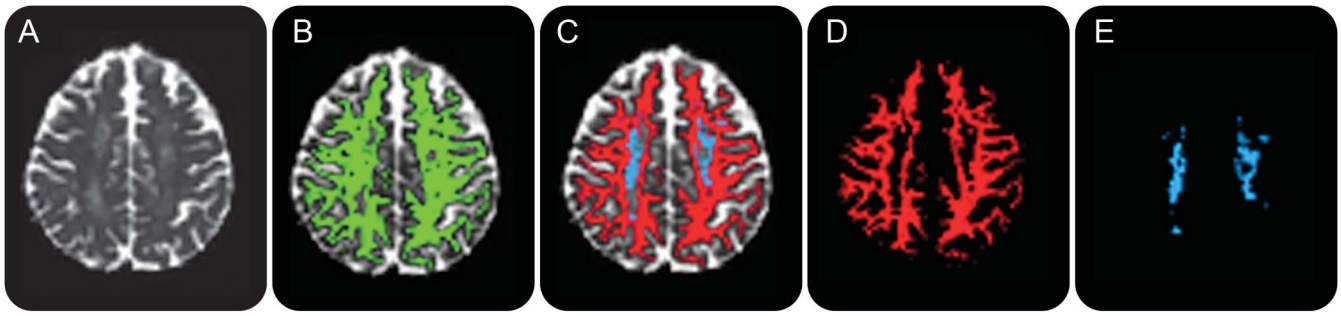

(A) Example of a mean diffusivity (MD) map from a participant with periventricular and deep white matter hyperintensities (WMHs). (B) The NAWM (green) is overlaid on the MD map. (C) Regions of positive cerebrovascular reactivity (CVR) (red) and negative CVR (steal physiology) in blue are overlaid on an MD map. (D) NAWM mask with only regions of positive CVR. (E) NAWM mask with only regions of negative CVR.

corrected using the Greenhouse-Geisser method. Results were considered significant and Bonferroni-corrected if the per-comparison p value was less than 0.05/(3 comparisons) = 0.0167.

RESULTS Reasons for clinic referral included transient episodes of paresthesia, chronic imbalance, gait disturbances, syncopal episodes, headaches, cognitive decline, or memory impairment. Participants had an average WMH volume of 28.5 (23.4) mL.

The mean (SD) for each MRI metric in each group is summarized in table e-1 at Neurology.org. Comparing NAWM with steal physiology (negative CVR) to NAWM with positive CVR (figure 4), FA decreased by 3.7% (2.4), MD significantly increased by 3.9% (3.1), CBF decreased by 22.1% (8.2), rCBV decreased by 22.2% (7.0), and Tmax increased by 10.9% (13.2) (all $p < 0.01$; repeated-measures one-way ANOVA). MTT values did not significantly differ between NAWM with steal physiology CVR (3.9 [0.2] vs 4.0 [0.2] seconds; Friedman test). TTP values were not significant between NAWM with negative and positive CVR after correcting for the potentially confounding influence of spatial location (as described in Methods) (20.8 [0.7] vs 20.6 [0.7] seconds; repeated-measures one-way ANOVA).

DISCUSSION We found an association between impaired CVR (steal physiology) and abnormal diffusion and perfusion metrics in NAWM, in the absence of hemodynamically significant large vessel disease. Our findings demonstrate that NAWM may not be as normal as conventional MRI sequences would suggest. We found that some areas in NAWM show negative CVR, i.e., steal physiology,[28] a marker of cerebrovascular regulation dysfunction. Indeed, our finding of abnormal diffusion and perfusion MRI metrics in these areas is indicative of such dysfunction, and is consistent with animal models of chronic hypoperfusion, where chronically ischemic white matter demonstrates demyelination, axonal loss, and gliosis.[29] We therefore suggest that negative CVR is capable of detecting areas in the NAWM with subtle pathologic features indicating structural damage to white matter that resulted in increased water diffusivity. Other studies in humans have shown that steal physiology is associated with elevated white matter diffusivity in patients with intracranial[30] and extracranial[31] large artery stenoocclusive disease. After accounting for the confound of spatial location, there was no significant difference in T2 values between NAWM with negative and positive

Figure 3 Regions of interest used to assess the influence of spatial location on MRI metrics

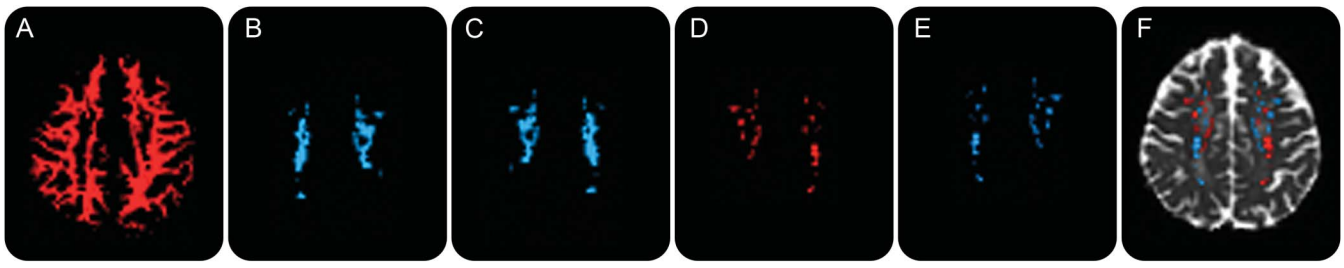

(A) Normal-appearing white matter (NAWM) mask with only regions of positive cerebrovascular reactivity (CVR). (B) NAWM mask with only regions of steal physiology (negative CVR). (C) Image B is left-right flipped about the y-axis in Montreal Neurologic Institute coordinates while retaining native structure. (D) Image C is overlaid on image A and overlapping voxels are retained, giving rise to a contralateral NAWM mask that has only positive CVR. (E) Image D is left-right flipped about the y-axis, giving rise to the original NAWM with steal physiology that also has contralateral positive CVR. (F) The 2 final masks, NAWM with steal physiology (E) and the corresponding contralateral homologous NAWM with positive CVR (D), are overlaid on a mean diffusivity map.

Figure 4 **Comparison of MRI metrics between regions of normal-appearing white matter (NAWM) with positive cerebrovascular reactivity (CVR) and steal physiology**

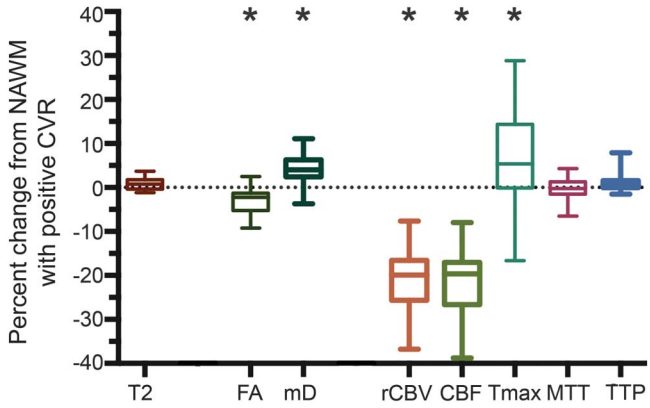

The values in MRI metrics are derived from paired comparisons of regions of positive CVR and their corresponding contralateral homologous regions of NAWM with steal physiology. Values are given as % change from NAWM with positive CVR. The regions of interest used for these measurements are taken from figure 3F, thereby accounting for differences in spatial location that may give rise to differences in MRI metrics. Fractional anisotropy (FA), cerebral blood flow (CBF), and relative cerebral blood volume (rCBV) values are significantly lower in NAWM with steal physiology compared to NAWM with positive CVR. Results from mean diffusivity (mD) and T2 metrics show significant increases in regions of steal physiology compared to NAWM with positive CVR. *Denotes significance compared to NAWM with positive CVR ($p < 0.01$). Bars indicate minimum and maximum, boxes indicate the interquartile range (25th–75th percentile), and the line within each box indicates the median. MTT = mean transit time; Tmax = time-to-maximum; TTP = time-to-peak.

CVR. This finding is not surprising as the definition of NAWM is made on T2-weighted images, so any significant increase in T2 would have been seen as an area of hyperintensity. Thus, changes in T2 are more likely to be associated with overt conversion of NAWM to WMH.

We also report an association between negative CVR and subtle abnormal perfusion metrics in NAWM. A previous study found NAWM CBF in participants with known WMHs to be reduced compared to controls (17.9 vs 21.6 mL/100 g/min, respectively).[32] Another study found the CBF of WMHs was 40% of that in healthy controls, but white matter CBV did not differ.[33] Although our CBF values are higher, values found in NAWM with negative CVR shifted towards those of WMHs; the mean (SD) NAWM CBF with negative CVR was 20.5 (0.9) compared to 26.4 (1.0) mL/100 g/min in the contralateral NAWM with positive CVR. In addition to CBF differences, CBV was reduced and Tmax was higher in NAWM with negative CVR compared to NAWM with positive CVR. These findings suggest that a loss in cerebrovascular regulation may precede the development of WMHs, and provide support for the theory that chronic hypoperfusion and the resulting ischemic damage may be the underlying pathophysiologic mechanism of age-related leukoaraiosis.

Our observations also raise the question whether all cerebral tissue with negative CVR is prone to pathologic changes. Steal physiology has been shown to be correlated with cortical thinning,[12] enhanced risk of stroke,[34] and cognitive decline[35] but has also been observed in the white matter of young healthy individuals.[27] The cortical thinning associated with impaired CVR in patients with unilateral steno-occlusive disease is consistent with the concept of progressive selective necrosis secondary to a mismatch between blood flow and increased axonal-glial activity in areas of maximum vasodilation (and therefore impaired CVR).[12] A reduction in the complexity of the neuropil without neuronal loss is also possible. Impaired CVR resulting in cortical thinning may occur in the absence of overt infarction. However, recent evidence has shown that accumulation of microinfarcts may lead to the development of WMHs.[36]

Recent research using transcranial Doppler ultrasound found that arterial stiffening reduces damping of the arterial waveform and increases cerebral pulsatility, which may damage small vessels, increase shear stress, and exacerbate impaired CVR.[37] Another factor influencing arterial pulsations, venous collagenosis, is a mechanical consequence of increased cerebral pulsatility and mechanical fatigue of vascular smooth muscles.[38] Increased arterial pulsations result in arteriolar myogenic fatigue, reduction in arteriolar myogenic tone, and abnormal penetration of the insufficiently dampened arterial pulse wave into the venules. The high pulsatile motion causes mechanical damage to the veins.[39] Collectively, these studies suggest that venous collagenosis, arterial stiffening, increased cerebral pulsatility, and impaired CVR may play a pathophysiologic role in developing leukoaraiosis.

Our methodologic approach, using CO_2 as a vasodilatory stimulus to assess cerebrovascular reactivity, must be considered carefully. In order to provide a consistent stress to the cerbrovasculature for each patient, the control of the $P_{ET}CO_2$ stimulus must be precise and repeatable. Intersubject variation in stimulus occurs in breath-holding or fixed inspired CO_2 concentration,[40] which would increase the variability of CVR and could have obscured the subtle changes observed in this study. Moreover, the stress must be sufficient to detect areas of reduced CVR.[11] This also cannot be guaranteed with breath-holding or fixed inspired CO_2 concentrations. In this study, participants were presented with a 10 mm Hg square wave increase in $P_{ET}CO_2$ that was sustained for at least 2 minutes, from an average baseline of 40 mm Hg, and so was able to detect negative CVR. Furthermore, we used a control system that was capable of producing an accurate quantitative $P_{ET}CO_2$ stimulus that controlled arterial PCO_2.[16] Thus we are confident that we have approached the limit of the autoregulatory capacity of the cerebral microvasculature and can accurately define

regions of pathologic steal, which demonstrate redistribution of blood flow to areas with positive CVR.

Our study was limited by several factors. First, our study involved 2 centers and only a subset (25 out of 75 participants) had perfusion imaging. Second, our study did not make a clear distinction between regions of ischemia or infarction and WMHs without ischemia. Although the WMHs in our study participants are of presumed ischemic origin given the study population and presence of vascular risk factors, the presence of other nonischemic causes of WMH in any given patient could not be definitively excluded by our imaging protocol.

We have shown that areas of NAWM that exhibit negative CVR (steal physiology) also show subtle changes in parameters describing tissue structure and perfusion, and that these parameters are shifted towards those seen in overt WMHs. These observations provide a new hypothesis regarding the underlying pathophysiology of the progression of NAWM to WMH. Although we detected subtle pathologic changes for several measures in NAWM exposed to steal physiology, it is uncertain whether these regions will ultimately develop into WMHs, and so this aspect requires further investigation in longitudinal studies.

AUTHOR CONTRIBUTIONS

All authors agreed to be accountable with regards to the accuracy and integrity of the work. All authors have critically revised the manuscript and approved the final manuscript to be published. Study concept and design: K.S., A.P.C., D.M.M., J.D., J.A.F., S.E.B., and D.J.M. Acquisition of data: K.S. and O.S. Data analysis and interpretation: K.S., B.P., J.C., J.P., A.P.C., D.M.M., L.V., J.D., J.A.F., S.E.B., and D.J.M. Statistical plan and analysis: K.S., J.C., and A.P.C. Obtained funding: L.V., J.A.F., S.E.B., and D.J.M.

ACKNOWLEDGMENT

The authors thank the Toronto Western Hospital and Sunnybrook Health Sciences Centre RespirAct technologists, Anne Battisti-Charbonney and Diem Pham, as well as the MRI technologists, Keith Ta and Eugen Hlasny; David Crane (MacIntosh laboratory manager) and Anoop Ganda (psychometrist/research coordinator) for enabling the Sunnybrook data acquisition; Alicia McNeely and Courtney Berezuk, Sunnybrook BrainLab imaging analysts, for identifying areas of white matter hyperintensities and lacunes for the Sunnybrook dataset; and Christopher Scott, Sunnybrook BrainLab manager, for facilitating training and analysis using the Lesion Explorer pipeline.

STUDY FUNDING

Financial support for this project was provided by the Canadian Stroke Network and the Ontario Research Fund (K.S., B.P., A.P.C., J.P., J.C., O.S., J.D., D.M.M., J.A.F., S.E.B., D.J.M.), the Alternate Funding Plan for the Academic Health Science Centre of Ontario Innovation Fund, and the Heart and Stroke Foundation Canadian Partnership for Stroke Recovery and LC Campbell Foundation (Sunnybrook Brain Lab).

DISCLOSURE

K. Sam, B. Peltenburg, J. Conklin, O. Sobczyk, J. Poublanc, A. Crawley, D. Mandell, and L. Venkatraghavan report no disclosures relevant to the manuscript. J. Duffin is a shareholder in Thornhill Research Inc. J. Fisher is a coinventor of the RespirAct, a device used in this study. He also holds shares and serves as a director of Thornhill Research Inc., a University of Toronto/University Health Network-related company, which retains an ownership position and will receive royalties should the RespirAct become a commercial product. S. Black has received compensation in the past 2 years for ad hoc consulting with Novartis. Pfizer, Eli Lilly, and Richard Lewar Centre of Excellence in Cardiovascular Research. Her research unit is receiving contract research funding from Roche, GE Healthcare, Eli Lilly, Avid, Pfizer, Lundbeck, and Elan. Dr. Black also receives research funding from CIHR, NIH, Heart and Stroke Foundation of Canada, Alzheimer Drug Discovery Foundation, Weston Foundation, Brain Canada, University of Toronto Department of Medicine, and the Ontario Brain Institute. D. Mikulis is a coinventor of the RespirAct, a device used in this study, holds a minor equity position in Thornhill Research Inc., and has received research support from GE Healthcare, Siemens, Toshiba, and the Ontario Research Fund. Go to Neurology.org for full disclosures.

Received September 28, 2015. Accepted in final form August 24, 2016.

REFERENCES

1. Moody DM, Brown WR, Challa VR, Ghazi-Birry HS, Reboussin DM. Cerebral microvascular alterations in aging, leukoaraiosis, and Alzheimer's disease. Ann NY Acad Sci 1997;826:103–116.
2. Wardlaw JM, Smith C, Dichgans M. Mechanisms of sporadic cerebral small vessel disease: insights from neuroimaging. Lancet Neurol 2013;12:483–497.
3. Verdelho A, Madureira S, Moleiro C, et al. White matter changes and diabetes predict cognitive decline in the elderly: the LADIS study. Neurology 2010;75:160–167.
4. Simoni M, Li L, Paul NL, et al. Age- and sex-specific rates of leukoaraiosis in TIA and stroke patients: population-based study. Neurology 2012;79:1215–1222.
5. Whitman GT, Tang Y, Lin A, Baloh RW. A prospective study of cerebral white matter abnormalities in older people with gait dysfunction. Neurology 2001;57:990–994.
6. de Leeuw FE, de Groot JC, Achten E, et al. Prevalence of cerebral white matter lesions in elderly people: a population based magnetic resonance imaging study: The Rotterdam Scan Study. J Neurol Neurosurg Psychiatry 2001;70:9–14.
7. Launer LJ, Berger K, Breteler MM, et al. Regional variability in the prevalence of cerebral white matter lesions: an MRI study in 9 European countries (CASCADE). Neuroepidemiology 2006;26:23–29.
8. van Dijk EJ, Prins ND, Vrooman HA, et al. Progression of cerebral small vessel disease in relation to risk factors and cognitive consequences: Rotterdam Scan Study. Stroke 2008;39:2712–2719.
9. Prins ND, Scheltens P. White matter hyperintensities, cognitive impairment and dementia: an update. Nat Rev Neurol 2015;11:157–165.
10. Black S, Gao F, Bilbao J. Understanding white matter disease: imaging-pathological correlations in vascular cognitive impairment. Stroke 2009;40(3 suppl):S48–S52.
11. Sobczyk O, Battisti-Charbonney A, Fierstra J, et al. A conceptual model for CO(2)-induced redistribution of cerebral blood flow with experimental confirmation using BOLD MRI. Neuroimage 2014;92:56–68.
12. Fierstra J, Poublanc J, Han JS, et al. Steal physiology is spatially associated with cortical thinning. J Neurol Neurosurg Psychiatry 2010;81:290–293.
13. Fazekas F, Kleinert R, Offenbacher H, et al. Pathologic correlates of incidental MRI white matter signal hyperintensities. Neurology 1993;43:1683–1689.
14. Han JS, Mikulis DJ, Mardimae A, et al. Measurement of cerebrovascular reactivity in pediatric patients with cerebral

vasculopathy using blood oxygen level-dependent MRI. Stroke 2011;42:1261–1269.
15. Kisilevsky M, Hudson C, Mardimae A, Wong T, Fisher J. Concentration-dependent vasoconstrictive effect of hyperoxia on hypercarbia-dilated retinal arterioles. Microvasc Res 2008;75:263–268.
16. Ito S, Mardimae A, Han J, et al. Non-invasive prospective targeting of arterial P(CO2) in subjects at rest. J Physiol 2008;586:3675–3682.
17. Vesely A, Sasano H, Volgyesi G, et al. MRI mapping of cerebrovascular reactivity using square wave changes in end-tidal PCO2. Magn Reson Med 2001;45:1011–1013.
18. Slessarev M, Han J, Mardimae A, et al. Prospective targeting and control of end-tidal CO2 and O2 concentrations. J Physiol 2007;581:1207–1219.
19. Cox RW. AFNI: software for analysis and visualization of functional magnetic resonance neuroimages. Comput Biomed Res 1996;29:162–173.
20. Miller AJ, Joseph PM. The use of power images to perform quantitative analysis on low SNR MR images. Magn Reson Imaging 1993;11:1051–1056.
21. Smith SM, Jenkinson M, Woolrich MW, et al. Advances in functional and structural MR image analysis and implementation as FSL. Neuroimage 2004;(23 suppl 1): S208–S219.
22. Smith SM. Fast robust automated brain extraction. Hum Brain Mapp 2002;17:143–155.
23. Kosior JC, Frayne R. PerfTool: a software platform for investigating bolus-tracking perfusion imaging quantification strategies. J Magn Reson Imaging 2007;25:653–659.
24. Smith MR, Lu H, Trochet S, Frayne R. Removing the effect of SVD algorithmic artifacts present in quantitative MR perfusion studies. Magn Reson Med 2004;51:631–634.
25. Ramirez J, Scott CJ, McNeely AA, et al. Lesion Explorer: a video-guided, standardized protocol for accurate and reliable MRI-derived volumetrics in Alzheimer's disease and normal elderly. J Vis Exp 2014.
26. Ramirez J, Gibson E, Quddus A, et al. Lesion explorer: a comprehensive segmentation and parcellation package to obtain regional volumetrics for subcortical hyperintensities and intracranial tissue. Neuroimage 2011;54:963–973.
27. Mandell DM, Han JS, Poublanc J, et al. Selective reduction of blood flow to white matter during hypercapnia corresponds with leukoaraiosis. Stroke 2008;39: 1993–1998.
28. Mandell DM, Han JS, Poublanc J, et al. Mapping cerebrovascular reactivity using blood oxygen level-dependent MRI in patients with arterial steno-occlusive disease: comparison with arterial spin labeling MRI. Stroke 2008;39: 2021–2028.
29. Hainsworth AH, Markus HS. Do in vivo experimental models reflect human cerebral small vessel disease? A systematic review. J Cereb Blood Flow Metab 2008;28: 1877–1891.
30. Conklin J, Fierstra J, Crawley AP, et al. Impaired cerebrovascular reactivity with steal phenomenon is associated with increased diffusion in white matter of patients with Moyamoya disease. Stroke 2010;41:1610–1616.
31. Conklin J, Fierstra J, Crawley AP, et al. Mapping white matter diffusion and cerebrovascular reactivity in carotid occlusive disease. Neurology 2011;77:431–438.
32. O'Sullivan M, Lythgoe DJ, Pereira AC, et al. Patterns of cerebral blood flow reduction in patients with ischemic leukoaraiosis. Neurology 2002;59:321–326.
33. Markus HS, Lythgoe DJ, Ostegaard L, O'Sullivan M, Williams SC. Reduced cerebral blood flow in white matter in ischaemic leukoaraiosis demonstrated using quantitative exogenous contrast based perfusion MRI. J Neurol Neurosurg Psychiatry 2000;69:48–53.
34. Markus H, Cullinane M. Severely impaired cerebrovascular reactivity predicts stroke and TIA risk in patients with carotid artery stenosis and occlusion. Brain 2001;124: 457–467.
35. Balucani C, Viticchi G, Falsetti L, Silvestrini M. Cerebral hemodynamics and cognitive performance in bilateral asymptomatic carotid stenosis. Neurology 2012;79: 1788–1795.
36. Conklin J, Silver FL, Mikulis DJ, Mandell DM. Are acute infarcts the cause of leukoaraiosis? Brain mapping for 16 consecutive weeks. Ann Neurol 2014;76:899–904.
37. Webb AJ, Simoni M, Mazzucco S, et al. Increased cerebral arterial pulsatility in patients with leukoaraiosis: arterial stiffness enhances transmission of aortic pulsatility. Stroke 2012;43:2631–2636.
38. Hayashi K, Mori K, Miyazaki H. Biomechanical response of femoral vein to chronic elevation of blood pressure in rabbits. Am J Physiol Heart Circ Physiol 2003;284:H511–H518.
39. Henry-Feugeas MC, Koskas P. Cerebral vascular aging: extending the concept of pulse wave encephalopathy through capillaries to the cerebral veins. Curr Aging Sci 2012;5:157–167.
40. Fisher JA. The CO_2 stimulus for cerebrovascular reactivity: fixing inspired concentrations vs targeting end-tidal partial pressures. J Cereb Blood Flow Metab 2016;36: 1004–1011.

Cerebrovascular reactivity and white matter integrity

Kevin Sam, Boris Peltenburg, John Conklin, et al.

Neurology 2016;87;2333-2339 Published Online before print October 28, 2016
DOI 10.1212/WNL.0000000000003373